Available online at www.sciencedirect.com
SCIENCE DIRECT
International Journal of Heat and Mass Transfer 49 (2006) 2381–2390
International Journal of HEAT and MASS TRANSFER
www.elsevier.com/locate/ijhmt

Heat transfer in parallel plates and circular porous passages with axial conduction

W.J. Minkowycz [a], A. Haji-Sheikh [b,*]

[a] Department of Mechanical and Industrial Engineering, University of Illinois at Chicago, Chicago, IL 60607-7022, United States
[b] Department of Mechanical and Aerospace Engineering, The University of Texas at Arlington, Arlington, TX 76019-0023, United States

Received 14 August 2005; received in revised form 28 October 2005
Available online 20 January 2006

Abstract

This study discusses the development of the exact series solutions for the computation of temperature in parallel plate and circular porous passages. These passages are filled with relatively high thermal conductivity materials; and therefore, this study includes the contribution of axial conduction. This leads to the solutions for a set of modified Graetz type problems for parallel plate channels and circular pipes. The numerical procedure yields the Nusselt number that indicates significant variations depending on the size of the Peclet. The Nusselt number is computed for selected values of the Peclet number, mainly, to demonstrate the mathematical and numerical procedure.
© 2005 Elsevier Ltd. All rights reserved.

1. Introduction

The placement of porous materials in flow passages can significantly enhance the heat transfer rate if the thermal conductivity of porous materials is sufficiently large. There has been a recent interest in using this concept for electronic cooling applications [1].

When the axial conduction is negligible, various studies are reported in the literature. Numerically developed solutions are in [2,3] and exact series solutions for different passages are in [4]. The use of Green's function is emphasized for parallel plate channels in [5] and for circular pipes in [6]. Also, for other passages, the method of weighted residuals in presented in [7].

The porous materials with relatively high thermal conductivity have small Peclet numbers and the contribution of axial conduction is significant. Nield et al. [8] numerically studied the contribution of axial conduction for flow through a porous medium located between two parallel plates. A similar study for flow through circular porous passages is in [9]. This study is devoted to the presentation of the exact series solutions for these flow passage by using a Graetz-type analysis to include the effect of axial conduction. The mathematical procedures using series solutions are similar to those in [5,6]; however, major numerical modifications are necessary.

2. Temperature fields in parallel plate channels

The first flow model considers a steady and hydrodynamically fully developed flow between two impermeable parallel plates, $2H$ apart (see Fig. 1). The Brinkman momentum equation describes the velocity in these channels

$$\mu_e \frac{\partial^2 u}{\partial y^2} - \frac{\mu}{K} u - \frac{\partial p}{\partial x} = 0, \tag{1}$$

where μ is the fluid viscosity, μ_e the effective viscosity, and K is the permeability. The solution of this equation is available in the literature, e.g., Ref. [4]. However, for completeness of this presentation, a brief description of the mathematical procedure is necessary. Assuming constant

* Corresponding author. Tel.: +1 817 272 2010; fax: +1 817 272 2952.
E-mail address: haji@mae.uta.edu (A. Haji-Sheikh).

0017-9310/$ - see front matter © 2005 Elsevier Ltd. All rights reserved.
doi:10.1016/j.ijheatmasstransfer.2005.10.032

Nomenclature

A	area, m^2
B_m	coefficient
Br	Brinkman number, $\mu U^2/[Dak_e(T_1 - T_2)]$
C	duct contour, m
c_n	coefficients
c_p	specific heat, J/kg K
Da	Darcy number, K/H^2 or K/r_o^2
D_h	hydraulic diameter, m
d_n	coefficients
F	pressure coefficient
f	Moody friction factor
h	heat transfer coefficient, W/m^2 K
$\bar{h}$	average heat transfer coefficient, W/m^2 K
i, j	indices
K	permeability, m^2
k_e	effective thermal conductivity
M	μ_e/μ
Nu_D	Nusselt number, hD_e/k
m, n	indices
p	pressure, Pa
Pe	Peclet number, $\rho c_p L_c U/k_e$
Pr	Prandtl number, $\mu c_p/k_e$
r	radial coordinate
r_o	pipe radius, m
S	volumetric heat source, W/m^3
T	temperature, K
T_i	temperature in region 1 or 2
T_w	wall temperature, K
u	velocity, m/s
$\bar{u}$	$\bar{u} = \mu u/(\Phi L_c^2)$
U	average velocity, m/s
$\overline{U}$	average value of $\bar{u}$
x	axial coordinate, m
$\bar{x}$	$x/(PeH)$ or $\bar{x} = x/(Per_o)$
y, z	coordinates, m
$\bar{y}, \bar{z}$	y/a and z/a

Greek symbols

β	coefficient, Eqs. (15b) or (35b)
Φ	$-\partial p/\partial x$
λ_m	eigenvalues
θ_i	$(T - T_i)/(T_1 - T_2)$, $i = 1$ or 2
μ	fluid viscosity, N s/m^2
μ_e	effective viscosity, N s/m^2
ψ	coefficient, Eqs. (15a) or (35a)
ρ	density, kg/m^3
η	y/H or r/r_o
ω	parameter, $1/\sqrt{MDa}$

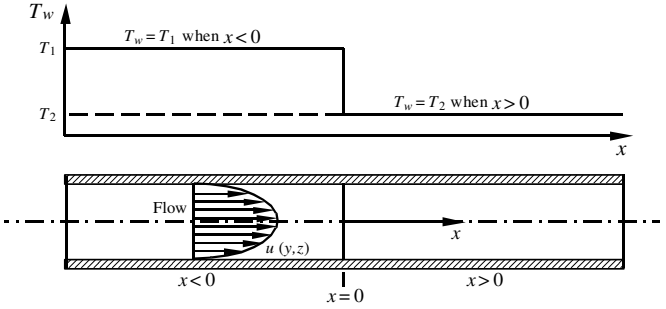

Fig. 1. Schematic of a duct with prescribed surface temperatures.

pressure gradient $\Phi = -\partial p/\partial x$, Eq. (1), in dimensionless form, reduces to an ordinary differential equation

$$M\frac{d\bar{u}}{d\bar{y}} - \frac{1}{Da}\bar{u} + 1 = 0, \tag{2}$$

where $\bar{y} = y/H$, $M = \mu_e/\mu$, $\bar{u} = \mu u/(\Phi H^2)$, and $Da = K/H^2$ is the Darcy number. The solution of Eq. (2) using the boundary conditions $\bar{u} = 0$ at $\bar{y} = 1$ and the symmetry condition $\partial\bar{u}/\partial\bar{y} = 0$ at $\bar{y} = 0$ is

$$\bar{u} = Da\left[1 - \frac{\cosh(\omega\bar{y})}{\cosh(\omega)}\right], \tag{3}$$

where $\omega = (MDa)^{-1/2}$. Then, the definition

$$\overline{U} = \int_0^1 \bar{u}\,d\bar{y} \tag{4}$$

leads to a relation for the reduced mean velocity $\overline{U}$ as

$$\overline{U} = Da[1 - \tanh(\omega)/\omega] \tag{5}$$

and

$$\frac{u}{U} = \frac{\bar{u}}{\overline{U}} = \frac{\omega}{\omega - \tanh(\omega)}\left[1 - \frac{\cosh(\omega\bar{y})}{\cosh(\omega)}\right]. \tag{6}$$

The temperature distribution assuming local thermal equilibrium is obtainable from the energy equation

$$u\frac{\partial T}{\partial x} = \frac{k}{\rho c_p}\left(\frac{\partial^2 T}{\partial x^2} + \frac{\partial^2 T}{\partial y^2}\right). \tag{7}$$

Introducing the Peclet number $Pe = \rho c_p\, HU/k$ where U is the mean velocity in the duct, and dimensionless $\bar{x} = x/(PeH)$, the energy equation, Eq. (7), reduces to

$$\frac{d^2T}{d\bar{y}^2} = \frac{u}{U}\frac{\partial T}{\partial \bar{x}} - \frac{1}{Pe^2}\frac{d^2T}{d\bar{x}^2}. \tag{8}$$

Often, there is an unheated section in a passage that is followed by the heated section as shown in Fig. 1. When T_1 and T_2 in Fig. 1 are constants, one can select two different dimensionless temperatures, $\theta_1 = (T - T_1)/(T_1 - T_2)$ when $x < 0$ and $\theta_2 = (T - T_2)/(T_1 - T_2)$ when $x > 0$ and the partial differential equation, Eq. (8), for these two regions takes the form

$$\frac{d^2\theta_i}{d\bar{y}^2} = \frac{u}{U}\frac{\partial\theta_i}{\partial\bar{x}} - \frac{1}{Pe^2}\frac{d^2\theta_i}{d\bar{x}^2} \quad \text{for } i = 1 \text{ or } 2. \tag{9}$$

The solution of the partial differential equation (9) is obtainable using the method of separation of variables by setting $\theta(\bar{x},\bar{y}) = X(\bar{x})Y(\bar{y})$. The substitution of this functional for θ in Eq. (9) yields

$$\frac{Y''}{Y} = \frac{u}{U}\frac{X'}{X} - \frac{1}{Pe^2}\frac{X''}{X}. \tag{10}$$

Because $u = u(y)$ on the right side of Eq. (10), it is possible to separate the variables if one considers the relation $X'(\bar{x}) = \lambda^2 X(\bar{x})$ and then differentiate it to get $X''(\bar{x}) = \lambda^2 X'(\bar{x}) = \lambda^4 X(\bar{x})$. This leads to the following differential equation for computation of $Y(\bar{y})$:

$$Y''(\bar{y}) - \lambda^2\left(\frac{u}{U}\right)Y(\bar{y}) + \frac{\lambda^4}{Pe^2}Y(\bar{y}) = 0. \tag{11}$$

The parameter λ is the eigenvalue in this equation and it is the solution of the differential equation $X'(\bar{x}) = \lambda^2 X(\bar{x})$; that is, $\exp(\lambda^2\bar{x})$. This methodology leads to the following temperature solutions,

$$\theta_i = \sum_{m=1}^{\infty} A_m e^{\lambda_m^2\bar{x}} Y_m(\bar{y}) \quad \text{for } i = 1 \text{ or } 2. \tag{12}$$

In this equation θ_1 is finite as $x \to -\infty$ and θ_2 is finite as $x \to +\infty$. Therefore, for $x < 0$, the eigenvalue λ in Eq. (11) is real. However, the coefficient λ in Eq. (11) becomes imaginary when $x > 0$. This leads to the following two relations in which λ_m^2 in real for both θ_1 and θ_2:

$$\theta_1 = \sum_{m=1}^{\infty} A_m Y_m(\bar{y}) e^{\lambda_m^2\bar{x}} \quad \text{when } x < 0 \tag{13a}$$

and

$$\theta_2 = \sum_{m=1}^{\infty} B_m Y_m(\bar{y}) e^{-\lambda_m^2\bar{x}} \quad \text{when } x > 0. \tag{13b}$$

Because the computation of θ_2 is the main objective of this study, Eq. (11) is utilized when λ is replaced with $i\lambda$. Once the value of u/U from Eq. (6) is placed in the modified Eq. (11), it becomes

$$Y''(\bar{y}) + \lambda^2\left\{\frac{\omega}{\omega - \tanh(\omega)}\left[1 - \frac{\cosh(\omega\bar{y})}{\cosh(\omega)}\right]\right\}Y(\bar{y}) + \frac{\lambda^4}{Pe^2}Y(\bar{y}) = 0. \tag{14}$$

Next, consideration is given to the exact and numerical solutions of this ordinary differential equation using a methodology similar that in [4]. For simplicity of this presentation, let

$$\psi = \frac{1}{\omega[\omega - \tanh(\omega)]} \tag{15a}$$

and

$$\beta = \frac{1}{\cosh(\omega)} \tag{15b}$$

then Eq. (14) reduces to

$$Y''(\bar{y}) + \{\lambda^4/Pe^2 + \omega^2\lambda^2\psi[1 - \beta\cosh(\omega\bar{y})]Y(\bar{y})\} = 0. \tag{16}$$

This differential equation has the form of a modified Mathieu differential equation [10] and the solution for this special Mathieu differential equation is described below.

Solution: The solution of Eq. (16) has a hypergeometric form

$$Y(\eta) = \sum_{n=0}^{\infty} c_n\eta^n, \tag{17}$$

wherein the independent variable $\eta = \bar{y} = y/H$. Following substitution $Y(y) = Y(\eta)$ from Eq. (17) in Eq. (16) and after removing the zero terms, the results is

$$\sum_{n=2}^{\infty} c_n n(n-1)\eta^{n-2} + \omega^2\lambda^2\psi[1 - \beta\cosh(\omega\eta)] \times \sum_{n=0}^{\infty} c_n\eta^n + (\lambda^4/Pe^2)\sum_{n=0}^{\infty} c_n\eta^n = 0. \tag{18}$$

Next, using the relation

$$\beta\cosh(\omega\eta) = \sum_{i=0}^{\infty} a_i\eta^i, \tag{19}$$

where

$$a_i = \begin{cases} \frac{\beta}{i!}(\omega)^i & \text{when } i \text{ is even,} \\ 0 & \text{when } i \text{ is odd,} \end{cases} \tag{20}$$

further reduces Eq. (18) and it can be written as

$$\sum_{n=2}^{\infty} c_n n(n-1)\eta^{n-2} + (\lambda^4/Pe^2 + \omega^2\lambda^4\psi) \times \sum_{n=0}^{\infty} c_n\eta^n - \omega^2\psi\sum_{n=0}^{\infty} d_n\eta^n = 0, \tag{21}$$

where

$$d_n = \sum_{j=0}^{n} c_j a_{n-j}. \tag{22}$$

The term that includes η^0 suggests $c_0 = \text{constant} = 1$ whereas the terms that include η^1 require $c_1 = 0$ because of symmetry at $y = 0$. Accordingly, all the terms with odd power vanish in this solution. When $n > 1$, the constants are obtainable from the recursive relationz

$$c_{n+2} = -\frac{\lambda^4 c_n/Pe^2 + \omega^2\lambda^2\psi(c_n - d_n)}{(n+2)^2 - (n+2)}. \tag{23}$$

When $Pe \to \infty$, this relation reduces to the form presented in [4].

Following the determination of c_n, Eq. (17) yields the solution for $Y(\bar{y})$ and the next step is the computation of

the eigenvalues. The eigencondition $Y(1)=0$ when $\bar{y}=\eta=1$ leads toward accomplishing the task of finding the eigenvalues. Once the mth eigenvalue is known, the function $Y_m(\bar{y})$ for the mth eigenvalue replaces $Y(\bar{y})$ in Eq. (17) for subsequent insertion in Eqs. (13a) and (13b). Following the computation of the eigenvalues, the thermal compatibility conditions at $x=0$ location would provide the constants A_m and B_m also for inclusion in Eqs. (13a) and (13b).

According to the definitions of $\theta_1=(T-T_1)/(T_1-T_2)$ and $\theta_2=(T-T_2)/(T_1-T_2)$, the first compatibility condition at $x=0$ is

$$\theta_2-\theta_1=(T-T_1)/(T_1-T_2)-(T-T_2)/(T_1-T_2)=1 \tag{24}$$

and the next compatibility condition is

$$\partial\theta_1/\partial\bar{x}|_{\bar{x}=0}=\partial\theta_2/\partial\bar{x}|_{\bar{x}=0}. \tag{25}$$

The method of determination of A_m and B_m using these compatibility conditions is combined with that for circular pipes and it is presented in a later section.

3. Temperature fields in circular pipes

The next presentation concerns the determination of temperature field in a fluid passing through a porous medium bounded by an impermeable circular wall. The mathematical procedure is similar to that described for the parallel plate channel. In cylindrical coordinates, the momentum equation is

$$\mu_e\left(\frac{\partial^2 u}{\partial r^2}+\frac{1}{r}\frac{\partial u}{\partial r}\right)-\frac{\mu}{K}u-\frac{\partial p}{\partial x}=0, \tag{26}$$

where r is the local radial coordinate and x is the axial coordinate. In the subsequent analyses, the characteristic length is r_o and the implemented dimensionless quantities are $\bar{r}=r/r_o$, $\bar{u}=\mu u/(\Phi r_o^2)$, $Da=K/r_o^2$, and $\omega=(MDa)^{-1/2}$. Then, the momentum equation becomes

$$M\left(\frac{\mathrm{d}^2\bar{u}}{\mathrm{d}\bar{r}^2}+\frac{1}{\bar{r}}\frac{\mathrm{d}\bar{u}}{\mathrm{d}\bar{r}}\right)-\frac{u}{Da}+1=0. \tag{27}$$

Using the boundary condition $\bar{u}=0$ at $\bar{r}=1$ and the condition $\partial\bar{u}/\partial\bar{r}=0$ at $\bar{r}=0$, the solution is

$$\bar{u}=Da\left[1-\frac{I_0(\omega\bar{y})}{I_0(\omega)}\right], \tag{28}$$

where $\omega=(MDa)^{-1/2}$. By definition, the mean velocity is

$$U=\frac{2}{r_o^2}\int_0^{r_o} ur\,\mathrm{d}r \tag{29}$$

and the velocity profile take the following form

$$\frac{u}{U}=\frac{\bar{u}}{\bar{U}}=\frac{\omega I_0(\omega)}{\omega I_0(\omega)-2I_1(\omega)}\left[1-\frac{I_0(\omega\bar{r})}{I_0(\omega)}\right]. \tag{30}$$

Because the velocity is fully developed, the steady-state form of the energy equation, in cylindrical coordinates, is

$$u\frac{\partial T}{\partial x}=\frac{k}{\rho c_p}\left(\frac{\partial^2 T}{\partial r^2}+\frac{1}{r}\frac{\partial T}{\partial r}+\frac{\partial^2 T}{\partial x^2}\right). \tag{31}$$

Defining the dimensionless temperature $\theta_i=(T-T_i)/(T_1-T_2)$ where $i=1$ or 2, one obtains

$$\frac{u}{U}\frac{\partial\theta_i}{\partial\bar{x}}=\frac{\partial^2\theta_i}{\partial\bar{r}^2}+\frac{1}{\bar{r}}\frac{\partial\theta_i}{\partial\bar{r}}+\frac{1}{Pe^2}\frac{\partial^2\theta_i}{\partial\bar{x}^2}, \tag{32}$$

where $\bar{x}=x/(Per_o)$ and $Pe=\rho c_p r_o U/k$. To use the method of separation of variables, let $\theta_1(\bar{x},\bar{r})=R(\bar{r})\exp(\lambda^2\bar{x})$ and following its insertion in Eq. (32), one obtains

$$R''(\bar{r})+\frac{1}{\bar{r}}R'(\bar{r})-\lambda^2\left(\frac{u}{U}\right)R(\bar{r})+\left(\frac{\lambda^4}{Pe^2}\right)R(\bar{r})=0, \tag{33}$$

where λ is real when $x<0$ and imaginary for $x>0$.

The next task is the determination of the function $R(\bar{r})$ with emphasis on θ_2. The parameter λ in Eq. (33) serves as the eigenvalues. Eq. (33) after substituting for u/U and replacing λ with λi becomes

$$R''(\bar{r})+\frac{1}{\bar{r}}R'(\bar{r})+\lambda^2\left\{\frac{\omega I_0(\omega)}{\omega I_0(\omega)-2I_1(\omega)}\left[1-\frac{I_0(\omega\bar{r})}{I_0(\omega)}\right]\right\}R(\bar{r})+\left(\frac{\lambda^4}{Pe^2}\right)R(\bar{r})=0. \tag{34}$$

Using the abbreviations

$$\psi=\frac{I_0(\omega)}{\omega I_0(\omega)-2I_1(\omega)}\frac{1}{\omega} \tag{35a}$$

and

$$\beta=1/I_0(\omega). \tag{35b}$$

Eq. (34) becomes

$$R''(\bar{r})+\frac{1}{\bar{r}}R'(\bar{r})+\omega^2\lambda^2\psi[1-\beta I_0(\omega\bar{r})]R(\bar{r})+\lambda^4R(\bar{r})/Pe^2=0. \tag{35c}$$

The solution to Eq. (35c) should satisfy the boundary conditions $R'(0)=R(1)=0$. The derivation of an exact series solution for Eq. (35c) is presented below and the procedure is similar to that in [4] or [6].

Solution: To obtain the solution, let $\eta=\bar{r}=r/r_o$ and then set

$$R(\eta)=\sum_{n=0}^{\infty}c_n\eta^n \tag{36}$$

then

$$\frac{\mathrm{d}R(\eta)}{\mathrm{d}\eta}=\sum_{n=0}^{\infty}c_n n\eta^{n-1}\quad\text{for } n>0 \tag{37a}$$

and

$$\frac{\mathrm{d}^2R(\eta)}{\mathrm{d}\eta^2}=\sum_{n=0}^{\infty}c_n n(n-1)\eta^{n-2}\quad\text{for } n>1. \tag{37b}$$

After removing the zero terms in Eqs. (37a) and (37b), the substitution $R(\eta)$ and its derivatives in Eq. (35c) yields

$$\sum_{n=2}^{\infty} c_n n(n-1)\eta^n + \sum_{n=1}^{\infty} c_n n\eta^n + (\omega\eta)^2\lambda^2\psi \times [1-\beta I_0(\omega\eta)]\sum_{n=0}^{\infty} c_n\eta^n + \frac{\eta^2\lambda^4}{Pe^2}\sum_{n=0}^{\infty} c_n\eta^n = 0. \quad (38)$$

Following substitution for:

$$\beta I_0(\omega\eta) = \sum_{i=0}^{\infty} a_i\eta^i. \quad (39)$$

Eq. (38) can be written as

$$\sum_{n=2}^{\infty} c_n n(n-1)\eta^n + \sum_{n=1}^{\infty} c_n n\eta^n + \omega^2\lambda^2\psi \times \sum_{n=0}^{\infty} c_n\eta^{n+2} - \omega^2\lambda^2\psi \times \sum_{n=0}^{\infty} d_n\eta^{n+2} + \frac{\lambda^4}{Pe^2}\sum_{n=0}^{\infty} c_n\eta^{n+2} = 0, \quad (40a)$$

where

$$d_n = \sum_{j=0}^{n} c_j a_{n-j} \quad (40b)$$

and

$$a_i = \frac{\beta}{(i!)^2}\left(\frac{\omega}{2}\right)^{2i}. \quad (40c)$$

The term that includes η^0 suggests $c_0 = \text{constant} = 1$ whereas the terms that include η^1 require $c_1 = 0$. Accordingly, all the terms with odd powers vanish in the solution. The values of other constants are obtainable from the recursive relation

$$c_{n+2} = -\frac{\lambda^4 c_n/Pe^2 + \omega^2\lambda^2\psi(c_n + d_n)}{(n+2)^2}. \quad (41)$$

As $Pe \to \infty$, this equation reduces to the form presented in [4].

As for the previous case, the solution for $R_m(\bar{r})$ must satisfy the eigencondition $R_m(1) = 0$ when $\bar{r} = \eta = 1$. This condition leads toward the computation of eigenvalues and the function $R_m(\bar{r})$ describes the function $R(\bar{r})$ for the mth eigenvalue; that is, when $\lambda = \lambda_m$. The final temperature solutions, after the computation of eigenvalues, has the form

$$\theta_1 = \sum_{m=1}^{\infty} A_m R_m(\bar{r}) e^{\lambda_m^2\bar{x}} \quad \text{when } x < 0 \quad (42a)$$

and

$$\theta_2 = \sum_{m=1}^{\infty} B_m R_m(\bar{r}) e^{-\lambda_m^2\bar{x}} \quad \text{when } x > 0. \quad (42b)$$

To compute A_m or B_m for inclusion in Eqs. (42a) and (42b), one needs to use the compatibility thermal conditions as given by Eqs. (24) and (25). The method of determination of coefficients A_m or B_m for circular pipes is similar to that for parallel plate channels; therefore, they are combined in the following section.

4. Orthogonality condition and the determination of coefficients

The methodology presented in this section is similar to that in [11,12]. The modified formulations, presented here, are to assure the completeness of this presentation. Using the eigenvalues λ_m^2 and λ_n^2 in Eq. (11) or (33), the differential equation for both parallel plate and circular passages may be written as

$$\frac{1}{\eta^e}\frac{d}{d\eta}\left[\eta^e\frac{d\psi_m(\eta)}{d\eta}\right] + \lambda_m^2\left[\frac{\lambda_m^2}{Pe^2} - \frac{u(\eta)}{U}\right]\psi_m(\eta) = 0, \quad (43a)$$

$$\frac{1}{\eta^e}\frac{d}{d\eta}\left[\eta^e\frac{d\psi_n(\eta)}{d\eta}\right] + \lambda_n^2\left[\frac{\lambda_n^2}{Pe^2} - \frac{u(\eta)}{U}\right]\psi_n(\eta) = 0. \quad (43b)$$

In these two relations ψ stands for Y in Eq. (11) for parallel plate channels if the exponent e assumes a value of 0 and ψ stands for R in Eq. (33) for circular pipes if $e = 1$. Eqs. (43a) and (43b) may be written as

$$\frac{1}{\eta^e}\frac{d}{d\eta}\left[\eta^e\frac{d\psi_m(\eta)}{d\eta}\right] + \lambda_m^2\left[\frac{\lambda_m^2 + \lambda_n^2}{Pe^2} - \frac{u(\eta)}{U}\right]\psi_m(\eta) - \frac{\lambda_m^2\lambda_n^2}{Pe^2}\psi_m(\eta) = 0, \quad (44a)$$

$$\frac{1}{\eta^e}\frac{d}{d\eta}\left[\eta^e\frac{d\psi_n(\eta)}{d\eta}\right] + \lambda_n^2\left[\frac{\lambda_m^2 + \lambda_n^2}{Pe^2} - \frac{u(\eta)}{U}\right]\psi_n(\eta) - \frac{\lambda_m^2\lambda_n^2}{Pe^2}\psi_n(\eta) = 0 \quad (44b)$$

by adding and subtracting the last terms in these equations. Multiply both sides of Eq. (44a) by $\eta^e\psi_n(\eta)$ and both sides of Eq. (44b) by $\eta^e\psi_m(\eta)$ and then subtracting the resulting relations would leads to

$$\psi_n(\eta)\frac{d}{d\eta}\left[\eta^e\frac{d\psi_m(\eta)}{d\eta}\right] - \psi_m(\eta)\frac{d}{d\eta}\left[\eta^e\frac{d\psi_n(\eta)}{d\eta}\right] + (\lambda_m^2 - \lambda_n^2)\left[\frac{\lambda_m^2 + \lambda_n^2}{Pe^2} - \frac{u(\eta)}{U}\right]\eta^e\psi_n(\eta)\psi_m(\eta) = 0.$$

The integration of this equation from 0 to 1 and then integrating the first two terms by parts yields,

$$(\lambda_m^2 - \lambda_n^2)\int_0^1\left[\frac{\lambda_m^2 + \lambda_n^2}{Pe^2} - \frac{u(\eta)}{U}\right]r^e\psi_n(\eta)\psi_m(\eta)\,d\eta = 0. \quad (45a)$$

Therefore, the orthogonality condition is

$$\int_0^1\left[\frac{\lambda_m^2 + \lambda_n^2}{Pe^2} - \frac{u(\eta)}{U}\right]\psi_n(\eta)\psi_m(\eta)\eta^e\,d\eta = \begin{cases} 0 & \text{when } n \neq m \\ N_m & \text{when } n = m \end{cases} \quad (45b)$$

for parallel plate channels when $e = 0$ and for circular pipes when $e = 1$, as stated earlier.

This orthogonality condition is to be used to compute the coefficients A_m and B_m from the compatibility condition given by Eqs. (24) and (25). Because the eigenfunctions and the eigenvalues in $x+$ side and $x-$ side appear in different

summations, it is appropriate to identify θ_1 and θ_2 by using different symbols, e.g., when $x < 0$

$$\theta_1 = \sum_{m=1}^{\infty} A_m f_m(\eta) e^{\beta_m^2 \bar{x}} \quad \text{with } \beta_m^2 > 0 \tag{46a}$$

and when $x > 0$

$$\theta_2 = \sum_{m=1}^{\infty} B_m g_m(\eta) e^{-\lambda_m^2 \bar{x}} \quad \text{with } \lambda_m^2 > 0. \tag{46b}$$

The eigenfunctions $f_m(\eta)$ and $g_m(\eta)$ in Eqs. (46a) and (46b) are solutions of the following differential equations:

$$\frac{d}{d\eta}\left[\eta^e \frac{df_m(\eta)}{d\eta}\right] + \beta_m^2 \left[\frac{\beta_m^2}{Pe^2} - \frac{u(\eta)}{U}\right] f_m(\eta)\eta^e = 0, \tag{47a}$$

$$\frac{d}{d\eta}\left[\eta^e \frac{dg_n(\eta)}{d\eta}\right] + \lambda_n^2 \left[\frac{\lambda_n^2}{Pe^2} + \frac{u(\eta)}{U}\right] g_n(\eta)\eta^e = 0. \tag{47b}$$

The substitution of θ_1 and θ_2 from Eqs. (46a) and (46b) into Eqs. (24) and (25) leads to the relations for the determination of the coefficients A_m and B_m. The condition $\theta_1 = \theta_2$ at $x = 0$ yields

$$\sum_{m=1}^{\infty} B_m g_m(\eta) = 1 + \sum_{m=1}^{\infty} A_m f_m(\eta) \tag{48a}$$

and the relation $\partial\theta_1/\partial\bar{x}|_{\bar{x}=0} = \partial\theta_2/\partial\bar{x}|_{\bar{x}=0}$ yields

$$\sum_{m=1}^{\infty} -\lambda_m^2 B_m g_m(\eta) = \sum_{m=1}^{\infty} \beta_m^2 A_m f_m(\eta). \tag{48b}$$

Following the application of the orthogonality condition and other algebraic manipulations in [11,12], the coefficients are

$$A_n = \frac{\int_0^1 \left[\frac{\beta_n^2}{Pe^2} + \frac{u(\eta)}{U}\right] f_n(\eta)\eta^e \, d\eta}{\int_0^1 \left[\frac{2\beta_n^2}{Pe^2} + \frac{u(\eta)}{U}\right] f_n^2(\eta)\eta^e \, d\eta} \tag{49a}$$

that becomes

$$A_n = \frac{2}{\beta_n} \frac{1}{[df_n(\eta)/d\beta_n]_{\eta=1}} \tag{49b}$$

and

$$B_n = \frac{\int_0^1 \left[\frac{\lambda_n^2}{Pe^2} + \frac{u(\eta)}{U}\right] g_n(\eta)\eta^e \, d\eta}{\int_0^1 \left[\frac{2\lambda_n^2}{Pe^2} + \frac{u(\eta)}{U}\right] g_n^2(\eta)\eta^e \, d\eta} \tag{50a}$$

that becomes

$$B_n = -\frac{2}{\lambda_n} \frac{1}{[dg_n(\eta)/d\lambda_n]_{\eta=1}}. \tag{50b}$$

It is remarkable that A_n, Eq. (49b), depends only on the parameters within the θ_1 solution and B_n, Eq. (50b), depends only on the parameters within the θ_2 solution.

The temperature solution, using the aforementioned exact analysis provided accurate results when x is relatively large. However, the solution may require many eigenvalues at small values of $\bar{x}$. Once the temperature solution is known, the heat transfer coefficient $h = q_w/(T_2 - T_b)$ is obtainable following the determination of wall heat flux $q_w = (\partial T/\partial r)|_{r=r_o}$ and the bulk temperature T_b. It can be written in dimensionless form as

$$Nu = hL_c/k_e = -\frac{1}{\theta_b} \sum_{m=1}^{\infty} B_m \left.\frac{d\psi(\eta)}{d\eta}\right|_{\eta=1} e^{-\lambda_m^2 \bar{x}}, \tag{51}$$

where

$$\begin{aligned}\theta_b &= \frac{T_b - T_2}{T_1 - T_2} \\ &= (1+e) \sum_{m=1}^{\infty} B_m e^{-\lambda_m^2} \int_0^1 \left(\frac{u}{U}\right) \psi_m(\eta)\eta^e \, d\eta \\ &= (1+e) \sum_{m=1}^{\infty} B_m e^{-\lambda_m^2} \left[-\frac{\lambda_m^2}{Pe^2} \int_0^1 \psi_m \eta^e \, d\eta - \frac{1}{\lambda_m^2} \left.\frac{d\psi(\eta)}{d\eta}\right|_{\eta=1}\right].\end{aligned} \tag{52}$$

As stated earlier, for parallel plate channels, the parameter $e = 0$ and $\psi_m(\eta)$ stands for $Y_m(\bar{y})$ in Eq. (13b). For circular pipes, the parameter $e = 1$ and $\psi_m(\eta)$ stands for $R_m(\bar{y})$ in Eq. (42b) while θ_b stands for $\theta_{2,b}$.

5. Numerical studies

This numerical study evaluates the exact series solution in the presence of axial conduction for each case mentioned earlier. Three different *MDa* values are selected, 1, 10^{-3}, and 10^{-5}. This will permit one to observe the influence of *Pe* at small, intermediate, and large values of *MDa*. For each *MDa* value, the data for *Pe* values of 1, 2, 5, 10, and ∞ are presented.

5.1. Parallel plate channels

For parallel plate channels, data are acquired for the Nusselt number $Nu = hH/k_e$ and the bulk temperature $\theta_b = (T_b - T_2)(T_1 - T_2)$ for three selected *MDa* values. It is customary to show the variation of Nusselt number as a function of $(x/H)/Pe$ while having *Pe* as a parameter. Fig. 2(a) shows the Nusselt number and Fig. 2(b) provides the bulk temperature as a function of $(x/H)/Pe$ for $MDa = 10^{-5}$. Similarly, Figs. 3(a and b) and 4(a and b) display the variation of the Nusselt number and the bulk temperature when $MDa = 10^{-3}$, and 1. It is to be noted that both values of *MDa* and θ_b are needed in order to determine the heat flux values at the wall; that is

$$\frac{q_w H}{k_e(T_2 - T_1)} = Nu \times \theta_b. \tag{53a}$$

5.2. Circular pipes

The data for circular pipes are also acquired for $Nu = hr_o/k_e$ and θ_b when $MDa = 10^{-5}$, 10^{-3}, and 1. Fig. 5(a) displays the variation of Nusselt number as a function of $(x/H)/Pe$ when $Pe = 1$, 2, 5, 10, and ∞ while Fig. 5(b)

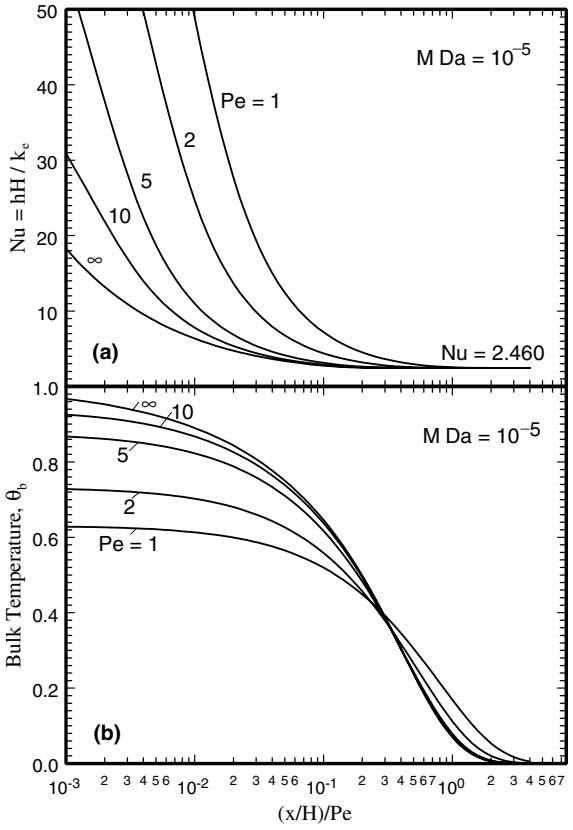

Fig. 2. Local Nusselt number and bulk temperature for parallel plate when $MDa = 10^{-5}$.

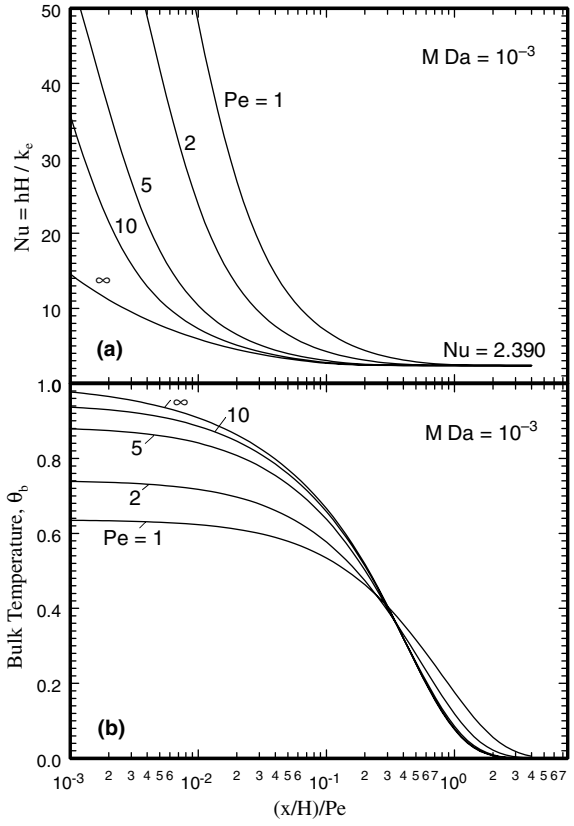

Fig. 3. Local Nusselt number and bulk temperature for parallel plate when $MDa = 10^{-3}$.

provides the corresponding values of the bulk temperature θ_b. Moreover, Figs. 6 and 7 demonstrate the influence of MDa values of 10^{-3} and 1, respectively. Again, the values of Nu and θ_b are needed in order to determine the heat flux values at the wall; that is

$$\frac{q_w r_o}{k_e(T_2 - T_1)} = Nu \times \theta_b. \tag{53b}$$

It is to be noted that for small values of Pe numbers, the spacing between the adjacent eigenvalues will reduce significantly. This indicates that a larger number of eigenvalues should be computed in order to achieve a desired accuracy. Table 1 is an illustration of this phenomenon for parallel plate channels wherein the first 15 eigenvalues are listed when $MDa = 10^{-5}$. Table 2 shows a similar behavior for circular pipes. In each of these two tables, the eigenvalues for $Pe = \infty$, 5 and 1 are tabulated. Both λ_m and λ_m^2 are retained mainly to show when $Pe = \infty$, the spacing between λ_m values approaches π. However, as Pe decreases, the spacing between eigenvalues also decreases. When $Pe = 1$, the spacing between adjacent λ_m^2 values approaches π. This is expected because, when Pe is small, the term containing λ_m^4/Pe^2 in Eq. (11) or in Eq. (33) will begin to dominate instead of the term containing λ_m^2. Accordingly, as Pe decreases, it is necessary to compute a larger number of eigenvalues for a comparable accuracy. Accurate computation of eigenvalues is an essential part of this study. All computations were performed symbolically using Mathematica [13].

6. Discussion

In the aforementioned presentation, it is assumed that the effect of viscous dissipation is negligible. The method of including the effects of frictional heating is well known. This section discusses a few mathematical details mainly to complete this presentation. The energy equation for parallel plate channels become

$$k_e \frac{\partial^2 T_i}{\partial y^2} + \left[\frac{\mu u^2}{K} + \mu_e \left(\frac{\partial u}{\partial y}\right)^2\right] = Cu \frac{\partial T_i}{\partial x} - k_e \frac{\partial^2 T_i}{\partial x^2} \quad \text{for } i = 1 \text{ and } 2 \tag{54a}$$

that in dimensionless form becomes

$$\frac{d^2\theta_i}{d\bar{y}^2} + Br\left[\left(\frac{u}{U}\right)^2 + MDa\left(\frac{\partial(u/U)}{\partial \bar{y}}\right)^2\right] = \frac{u}{U}\frac{\partial \theta_i}{\partial \bar{x}} - \frac{1}{Pe^2}\frac{d^2\theta_i}{d\bar{x}^2} \quad \text{for } i = 1 \text{ and } 2, \tag{54b}$$

where $Br = \mu U^2/[Dak_e(T_1 - T_2)]$ is the Brinkman number. All the boundary conditions remain the same as those

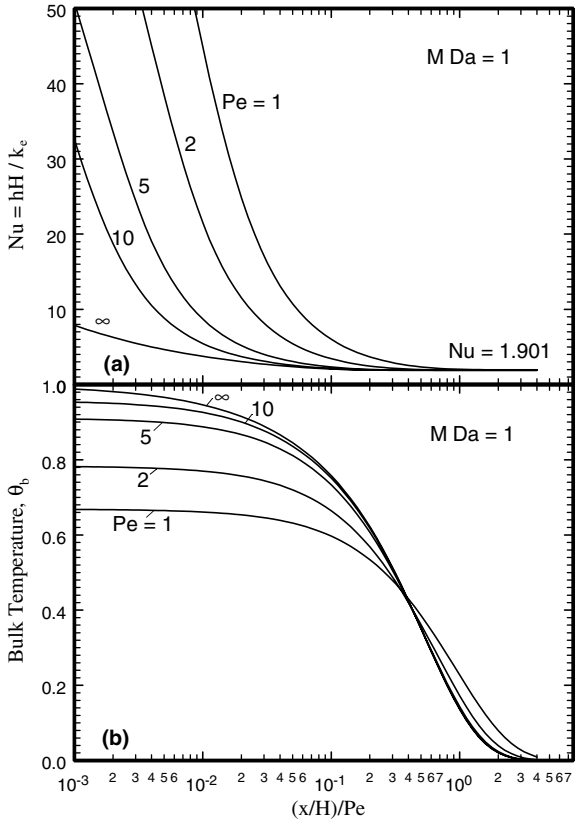

Fig. 4. Local Nusselt number and bulk temperature for parallel plate channels when $MDa = 1$.

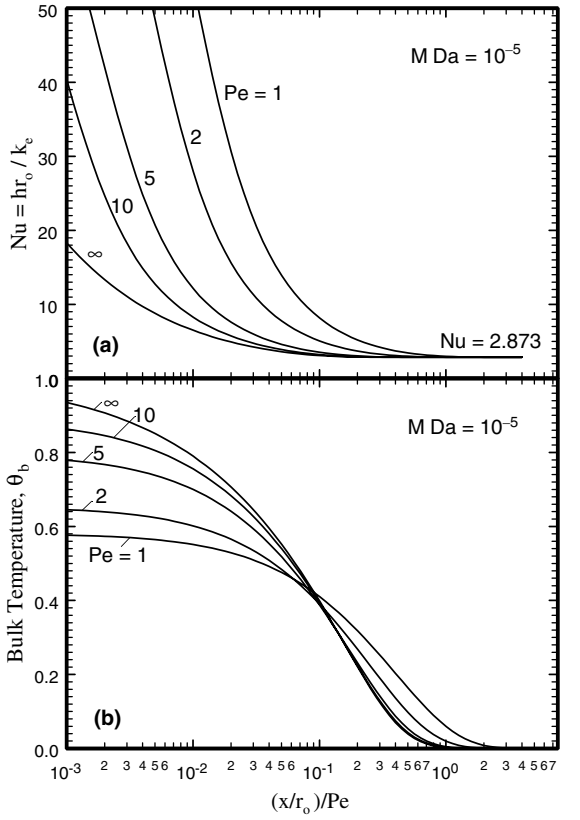

Fig. 5. Local Nusselt number and bulk temperature for circular pipes when $MDa = 10^{-5}$.

described earlier. The transformation to covert Eq. (54b) to Eq. (9) is readily available in [5, Eq. (32)]; it is

$$\theta_{i,s}(\bar{y}) = \frac{\omega^2}{4[\omega - \tanh(\omega)]^2}\{2\omega^2(1-\bar{y}^2) - 8[1 - \cosh(\omega\bar{y}) / \cosh(\omega)] + [\cosh(2\omega) - \cosh(2\omega\bar{y})]/\cosh^2(\omega)\}. \tag{55}$$

Therefore, adding $Br\theta_{i,s}(\bar{y})$, to $\theta_i(\bar{y},\bar{x})$ is required in order to include the effect of viscous dissipation and, subsequently, the application of the Fourier heat conduction at the wall leads to the relation

$$-\left.\frac{\partial\theta_{i,s}(\bar{y})}{\partial y}\right|_{\bar{y}=1} = \frac{\omega}{\omega - \tanh(\omega)} \tag{56}$$

that determines the contribution of frictional heating to the wall heat flux. As an example, for $MDa = 10^{-5}$, 10^{-3}, and 1, Eq. (56) yields $-\theta'_{i,s}(1) = 1.00317$, 1.03266, and 4.19453. The contribution of the viscous dissipation to the bulk temperature is readily available in [5, Eq. (30a)]

$$\theta_{b,s}(\omega) = \frac{\omega^2}{48}\left[\frac{1}{\omega\cosh(\omega) - \sinh(\omega)}\right]^3[(12\omega^3 - 150\omega) \times \cosh(\omega) + (4\omega^3 - 30\omega) \times \cosh(3\omega) + 57\sinh(\omega) + 41\sinh(3\omega)]. \tag{57}$$

Therefore, the dimensionless bulk temperature θ_b should be augmented by the quantity $Br\theta_{b,s}$. Similar equations, but with different forms are also available in [8]. For $MDa = 10^{-5}$, 10^{-3}, and 1 used in Figs. 2–4, Eq. (57) provides $\theta_{b,s} = 0.33649$, 0.36443, and 1.26162.

The process is similar for circular pipes. The governing diffusion equation in cylindrical coordinates is

$$k_e\frac{1}{r}\frac{\partial}{\partial r}\left(r\frac{\partial T_i}{\partial r}\right) + \left[\frac{\mu_e u^2}{K} + \mu_e\left(\frac{\partial u}{\partial r}\right)^2\right] = Cu\frac{\partial T_i}{\partial x} - k_e\frac{\partial^2 T_i}{\partial x^2} \quad \text{for } i = 1 \text{ and } 2 \tag{58a}$$

that in dimensionless form becomes

$$\frac{1}{\bar{r}}\frac{\partial}{\partial\bar{r}}\left(\bar{r}\frac{\partial\theta_i}{\partial\bar{r}}\right) + Br\left[\left(\frac{u}{U}\right)^2 + MDa\left(\frac{\partial(u/U)}{\partial\bar{r}}\right)^2\right] = \frac{u}{U}\frac{\partial\theta_i}{\partial\bar{x}} - \frac{1}{Pe^2}\frac{d^2\theta_i}{d\bar{x}^2} \quad \text{for } i = 1 \text{ and } 2. \tag{58b}$$

The transformation to covert this equation to the form of Eq. (32) without any changes in the boundary condition is readily available in [6, Eq. (43)]; it is $Br\theta_{i,s}$ where

$$\theta_{i,s}(\bar{r}) = \frac{1}{4[\omega - 2I_1(\omega)/I_0(\omega)]^2}\left\{6 - 8\left[\frac{I_0(\omega\bar{r})}{I_0(\omega)}\right] + 2\left[\frac{I_0(\omega\bar{r})}{I_0(\omega)}\right]^2 - \omega^2(1-\bar{r}^2)\right\}. \tag{59}$$

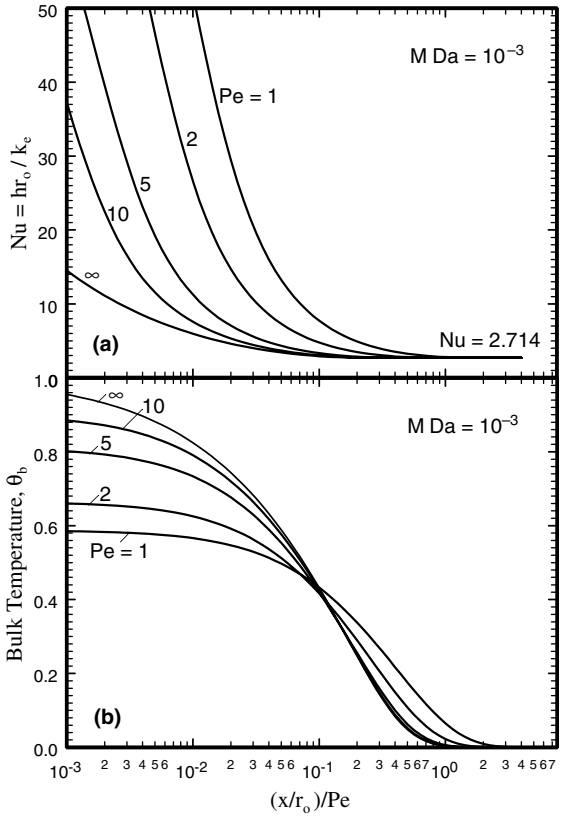

Fig. 6. Local Nusselt number and bulk temperature for circular pipes when $MDa = 10^{-3}$.

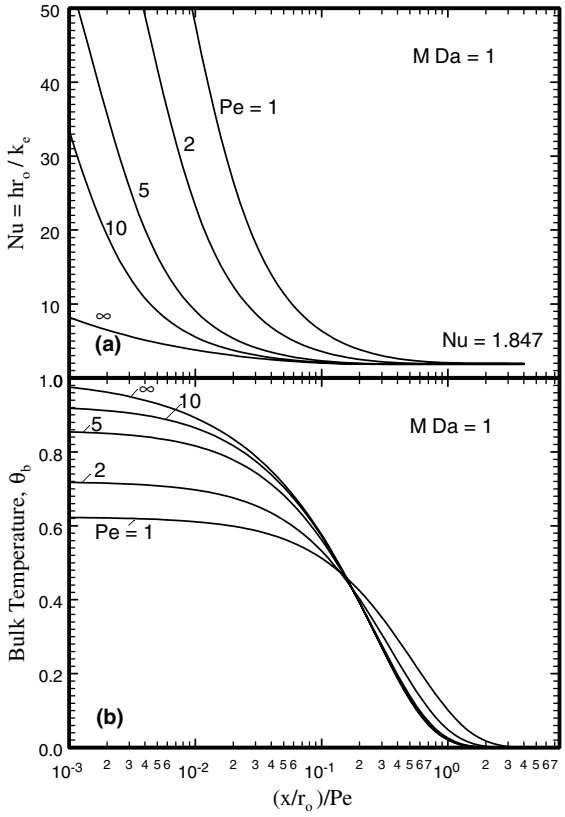

Fig. 7. Local Nusselt number and bulk temperature for circular pipes when $MDa = 1$.

As in the previous case, $-Br\partial\theta_{i,s}(\bar{r})/\partial\bar{r}|_{\bar{r}=1}$ yields the contribution of frictional heating to the wall heat flux where

$$-\partial\theta_{i,s}(\bar{r})/\partial\bar{r}|_{\bar{r}=1} = \frac{\omega^2 - 2I_1(\omega)/I_0(\omega)}{2[\omega - 2I_1(\omega)/I_0(\omega)]^2}. \tag{60}$$

For $MDa = 10^{-5}$, 10^{-3}, and 1 used in Figs. 5–7, Eq. (60) produces $-\theta'_{i,s}(1) = 0.50318$, 0.53318, and 4.66331. Finally, the dimensionless bulk temperature in circular pipes $\theta_{i,\mathrm{b}}$ must be augmented by the influence of frictional heating $Br\theta_{\mathrm{b},s}$ where [6, Eq. (38)].

$$\theta_{\mathrm{b},s} = \frac{\omega^2}{8[\omega - 2I_1(\omega)/I_0(\omega)]^3}\left\{\omega[(\omega^2 - 32) + 20I_1(\omega)^2/I_0(\omega)^2] + 4[(14 - \omega^2)I_1(\omega) + 2\omega I_2(\omega) + \omega^2 I_3(\omega)]/I_0(\omega) + 8\omega\int_0^1 [I_0(\omega\bar{r})/I_0(\omega)]^3\bar{r}\,\mathrm{d}\bar{r}\right\}. \tag{61}$$

For $MDa = 10^{-5}$, 10^{-3}, and 1, Eq. (61) yields $\theta_{\mathrm{b},s} =$ 0.12737, 0.14880, and 1.13609.

The influence of frictional heating for different Br values is well documented in [8,9] with graphical presentation of the data for parallel plate channels and circular pipes. For the data presented in Figs. 2–7, one can compute the Nusselt number that includes the contribution of frictional heating. Using the product of $Nu \times \theta_{\mathrm{b}}$ as given in Figs. 2–7, the relation

$$Nu_{\mathrm{total}} = \frac{Nu \times \theta_{\mathrm{b}} - Br \times \theta'_{1,s}(1)}{\theta_{\mathrm{b}} + Br \times \theta_{\mathrm{b},s}} \tag{62}$$

can provide the total effects due to wall temperature change and frictional heating. Test results indicate that they agree well with the reported data in [8,9]. However, there are some small differences mainly due to expected numerical errors from numerical computations. As an illustration, in the absence of axial conduction, the accuracy of the fully developed Nusselt number is directly related to the first eigenvalue, and the reported Nusselt numbers [8] for $MDa = 10^{-5}$ and 1 are $2hH/k_{\mathrm{e}} = 4.920$ and 3.806. These agree well with $2 \times 4.60 = 4.920$ and $2 \times 1.901 = 3.802$ taken from Figs. 2(a) and 4(a), respectively. This limiting value changes in the presence of frictional heating. Nield et al. [8] reports $2hH/k_{\mathrm{e}} = 6.641$ for $MDa = 1$ when using the viscous dissipation effect as given in [14]. For this case, Eq. (62) yields $2hH/k_{\mathrm{e}} = -2(\theta'_{2,s}(1)/\theta_{2,b}) = 2(4.19453/1.26162) = 6.649$.. Similarly, in the absence of frictional heating, for $MDa = 10^{-5}$ and 1, [9] reports $2hr_o/k_{\mathrm{e}} = 5.750$ and 3.958. These are in reasonably good agreement with $2 \times 2.873 = 5.746$ while there is a noticeable difference with $2 \times 1.847 = 3.694$ when using the data in Figs. 5(a) and 7(a),

Table 1
First 15 eigenvalues for a parallel plate channel when $MDa = 10^{-5}$

Eigenvalue no.	$Pe = 1$		$Pe = 5$		$Pe = \infty$	
	λ	λ^2	λ	λ^2	λ	λ^2
1	1.0711	1.1473	1.5022	2.2566	1.5683	2.4596
2	2.0585	4.2374	3.7618	14.1513	4.7049	22.1365
3	2.7145	7.3684	5.3557	28.6838	7.8416	61.4904
4	3.2412	10.5054	6.6220	43.8503	10.9783	120.5222
5	3.6938	13.6445	7.6974	59.2501	14.1150	199.2325
6	4.0969	16.7845	8.6464	74.7598	17.2517	297.6225
7	4.4637	19.9250	9.5042	90.3298	20.3886	415.6937
8	4.8027	23.0657	10.2925	105.9363	23.5255	553.4476
9	5.1192	26.2067	11.0257	121.5666	26.6624	710.8860
10	5.4174	29.3478	11.7138	137.2132	29.7995	888.0112
11	5.6999	32.4890	12.3641	152.8715	32.9367	1084.8251
12	5.9691	35.6303	12.9822	168.5385	36.0740	1301.3302
13	6.2267	38.7716	13.5725	184.2121	39.2113	1537.5291
14	6.4740	41.9130	14.1383	199.8908	42.3488	1793.4242
15	6.7123	45.0544	14.6824	215.5736	45.4865	2069.0181

Table 2
First 15 eigenvalues for a circular pipe when $MDa = 10^{-5}$

Eigenvalue no.	$Pe = 1$		$Pe = 5$		$Pe = \infty$	
	λ	λ^2	λ	λ^2	λ	λ^2
1	1.3978	1.9537	2.1960	4.8223	2.3972	5.7467
2	2.2449	5.0398	4.2134	17.7525	5.5026	30.2790
3	2.8575	8.1652	5.6992	32.4808	8.6264	74.4148
4	3.3614	11.2991	6.9069	47.7055	11.7543	138.1647
5	3.7995	14.4362	7.9453	63.1279	14.8839	221.5308
6	4.1922	17.5749	8.8684	78.6478	18.0143	324.5145
7	4.5513	20.7145	9.7068	94.2228	21.1452	447.1174
8	4.8841	23.8545	10.4801	109.8318	24.2764	589.3413
9	5.1957	26.9950	11.2010	125.4634	27.4078	751.1880
10	5.4896	30.1356	11.8790	141.1106	30.5395	932.6597
11	5.7686	33.2765	12.5207	156.7691	33.6713	1133.7585
12	6.0347	36.4174	13.1315	172.4361	36.8034	1354.4870
13	6.2896	39.5585	13.7153	188.1096	39.9355	1594.8475
14	6.5345	42.6997	14.2754	203.7881	43.0679	1854.8427
15	6.7706	45.8409	14.8145	219.4707	46.2004	2134.4753

respectively. In the presence of frictional heating, Ref. [9] reports $2hr_o/k_e = 8.206$ for $MDa = 1$ and the viscosity dissipation model in [14]. Using Eq. (62), and the procedure described earlier, this study yields $2hr_o/k_e = 2(4.66331/1.13609) = 8.209$.

7. Conclusion

The exact series solution permits one to compute temperature and heat flux with a high degree of accuracy. Therefore, such solutions are valuable for the purpose of verification of the numerical solutions. The data reported here indeed shows that the numerically acquired data in Nield et al. [8], for entrance flow problems in the presence of frictional heating and axial conduction for parallel plate channels, are sufficiently accurate. A similar conclusion was realized by comparing the present data with the graphical presentation in Kuznetsov et al. [9] for circular pipes.

References

[1] D.A. Nield, A. Bejan, Convection in Porous Media, second ed., Springer-Verlag, New York, 1999.
[2] D.A. Nield, A.V. Kuznetsov, M. Xiong, Thermally developing forced convection in a porous medium: parallel-plate channel or circular tube with walls at constant heat flux, Journal of Porous Media 6 (3) (2003) 203–212.
[3] D.A. Nield, A.V. Kuznetsov, M. Xiong, Thermally developing forced convection in a porous medium: parallel-plate channel or circular tube with isothermal walls, Journal of Porous Media 7 (1) (2004) 19–27.
[4] A. Haji-Sheikh, K. Vafai, Analysis of flow and heat transfer in porous media imbedded inside various-shaped ducts, International Journal of Heat and Mass Transfer 47 (8–9) (2004) 1889–1905.
[5] A. Haji-Sheikh, W.J. Minkowycz, E.M. Sparrow, Green's function solution of temperature field for flow in porous passages, International Journal of Heat and Mass Transfer 47 (22) (2004) 4685–4695.
[6] A. Haji-Sheikh, W.J. Minkowycz, E.M. Sparrow, A numerical study of the heat transfer to fluid flow through circular porous passages, Numerical Heat Transfer, Part A 46 (10) (2004) 929–956.
[7] A. Haji-Sheikh, E.M. Sparrow, W.J. Minkowycz, Heat transfer to flow through porous passages using extended weighted residuals method–A Green's function solution, International Journal of Heat and Mass Transfer 48 (7) (2005) 1330–1349.
[8] D.A. Nield, A.V. Kuznetsov, M. Xiong, Thermally developing forced convection in a porous medium: parallel plate channel with walls at uniform temperature, with axial conduction and viscous dissipation effects, International Journal of Heat and Mass Transfer 46 (4) (2003) 643–651.
[9] D.A. Nield, A.V. Kuznetsov, M. Xiong, Thermally developing forced convection in a porous medium: circular ducts with walls at constant temperature, with longitudinal conduction and viscous dissipation effects, Transport in Porous Media 53 (3) (2003) 331–345.
[10] N.W. McLachlan, Theory and Application of Mathieu Functions, Dover Publications, Inc., New York, 1964.
[11] J. Lahjomri, A. Oubarra, Analytical solution of the Graetz problem with axial conduction, Journal of Heat Transfer 121 (4) (1999) 1078–1083.
[12] J. Lahjomri, A. Oubarra, A. Alemany, Heat transfer by laminar Hartmann flow in thermal entrance region with a step change in wall temperature: the Graetz problem extended, International Journal of Heat and Mass Transfer 45 (5) (2002) 643–651.
[13] S. Wolfram, The Mathematica Book, fourth ed., Cambridge University Press, Cambridge, UK, 1999.
[14] A.K. Al-Hadhrami, L. Elliot, D.B. Ingham, A new model for viscous dissipation in porous media across a range of permeability values, Transport in Porous Media 53 (1) (2003) 117–122.